

Weakly Supervised Invariant Representation Learning Via Disentangling Known and Unknown Nuisance Factors

Jiageng Zhu^{1,2,3}, Hanchen Xie^{2,3}, and Wael Abd-Almageed^{1,2,3}

¹ USC Ming Hsieh Department of Electrical and Computer Engineering

² USC Information Sciences Institute

³ Visual Intelligence and Multimedia Analytics Laboratory

{jiagengz, hanchenx, wamageed}@isi.edu

Abstract. Disentangled and invariant representations are two critical goals of representation learning and many approaches have been proposed to achieve either one of them. However, those two goals are actually complementary to each other so that we propose a framework to accomplish both of them simultaneously. We introduce a weakly supervised signal to learn disentangled representation which consists of three splits containing predictive, known nuisance and unknown nuisance information respectively. Furthermore, we incorporate contrastive method to enforce representation invariance. Experiments shows that the proposed method outperforms state-of-the-art (SOTA) methods on four standard benchmarks and shows that the proposed method can have better adversarial defense ability comparing to other methods without adversarial training.

1 Introduction

Robust representation learning which aims at preventing overfitting and increasing generality can benefit various down-stream tasks [12,17,29]. Typically, a DNN learns to encode a representation which contains all factors of variations of data, such as pose, expression, illumination, and age for face recognition, as well as other nuisance factors which are unknown or unlabelled. Disentangled representation learning and invariant representation learning are often used to address these challenges.

For disentangled representation learning, Bengio *et al.* [1] define disentangled representation which change in a given dimension corresponding to variation of one and only one generative factors of the input data. Although many unsupervised learning methods have been proposed [13,3,16], Locatello *et al.* [22] have shown both theoretically and empirically that the factor variants disentanglement is impossible without supervision or inductive bias. To this end, recent works have adopted the concept of semi-supervised learning [24] and weakly supervised learning [23]. On the other hand, Jaiswal *et al.* [14] take an invariant representation learning perspective in which they split representation z into two parts $z = [z_p, z_n]$, where z_p only contains predictive related information, and z_n merely contains nuisance factors.

Invariant representation learning aims to learn to encode predictive latent factors which are invariant to nuisance factors in inputs [32,14,25,26,28]. By removing information of nuisance factors, invariant representation learning achieves good performance

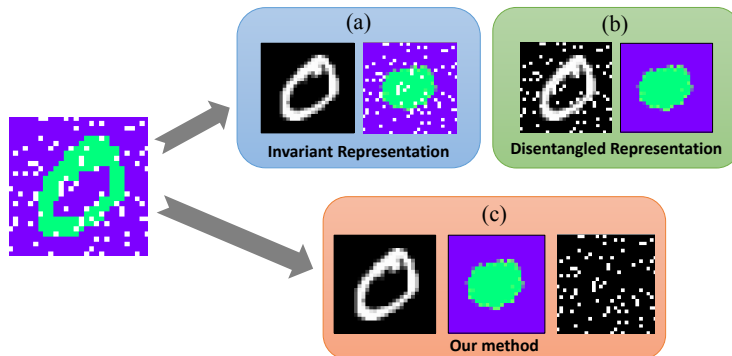


Fig. 1: Given an image with nuisance factors, (a): invariant representation learning splits predictive factors from all nuisance factors; (b): disentangled representation learning splits the known nuisance factors but leaving predictive and unknown nuisance factors; (c): Our method splits predictive, known nuisance and unknown nuisance factors simultaneously.

in challenges like adversarial attack [6] and out-of-distribution generalization [14]. Furthermore, invariant representation learning has also been studied in the reinforcement learning settings [5].

Despite the success of either disentangled or invariant representation learning methods, the relation between these two has not been thoroughly investigated. As shown in Figure 1(a), invariant representation learning methods learn representations that maximize prediction accuracy by separating predictive factors from all other nuisance factors, while leaving the representations of both known and unknown nuisance factors entangled. Meanwhile, as illustrated in Figure 1(b), although supervised disentangled representation methods can identify known nuisance factors, it fails to handle unknown nuisance factors, which may hurt downstream prediction tasks. Inspired by this observation, we propose a new training framework for seeking to achieve disentanglement and invariance of representation simultaneously. To split the known nuisance factors z_{nk} from predictive z_p and unknown nuisance factors z_{nu} , we introduce the weak supervision signals to achieve disentangled representation learning. To make predictive factors z_p independent of all nuisance factors z_n , we introduce a new invariant regularizer via reconstruction. The predictive factors from the same class are further aligned through contrastive loss to enforce invariance. Moreover, since our model achieve more robust representation comparing to other invariant models, our model is demonstrated to obtain better adversarial defense ability. In summary our main contributions are:

- Extending and combining both disentangled and invariant representation learning and proposing a novel approach to robust representation learning.
- Proposing a novel strategy for splitting the predictive, known nuisance factors and unknown nuisance factors, where mutual independence of those factors is achieved by the reconstruction step used during training.
- Outperforming state-of-the-art (SOTA) models on invariance tasks on standard benchmarks.

- Invariant latent representation trained using our method is also disentangled.
- Without using adversarial training, our model have better adversarial defense ability than other invariant models, which reflects that the generality of the model increases through our methods.

2 Related Work

Disentangled representation learning: Early works on disentangled representation learning aim at learning disentangled latent factors z by implementing an autoencoder framework [13,16,3]. Variational autoencoder (VAE) [17] is commonly used in disentanglement learning methods as basic framework. VAE uses DNN to map the high dimension input x to low dimension representation z . The latent representation z is then mapped to high dimension reconstruction \hat{x} . As shown in Equation (1), the overall objective function to train VAE is the evidence lower bounds (ELBO) of likelihood $\log p_\theta(x_1, x_2, \dots, x_n)$, which contains two parts: quality of reconstruction and Kullback-Leibler divergence (D_{KL}) between distribution $q_\phi(z|x)$ and the assumed prior $p(z)$. Then, VAE uses the negative of ELBO, $L_{VAE} = -ELBO$, as loss function to update the parameters in the model.

$$L_{VAE} = -ELBO = -\sum_{i=1}^N \left[\mathbb{E}_{q_\phi(z|x^{(i)})} [\log p_\theta(x^{(i)}|z)] - D_{KL}(q_\phi(z|x^{(i)})||p(z)) \right] \quad (1)$$

Advanced methods based on VAE improve the disentanglement performance by implementing new disentanglement regularization. β -VAE [13] modifies the original VAE by adding a hyper-parameter β to balance the weights of reconstruction loss and D_{KL} . When $\beta > 1$, the model gains stronger disentanglement regularization. **AnnealedVAE** implements a dynamic algorithm to change the β from large to small value during training. **FactorVAE** [16] proposes to use a discriminator in order to distinguish between the joint distribution of latent factors $q(z)$ and multiplication of marginal distribution of every latent factor $\prod q(z_i)$. By using the discriminator, **FactorVAE** can automatically finds a better balance between reconstruction quality and disentangled representation. Compared to β -VAE, **DIP-VAE** [18] adds another regularization $D(q_\phi(z)||p(z))$ between the marginal distribution of latent factors $q_\phi(z) = \int q_\phi(z|x)p(x)dx$ and the prior $p(z)$ to further aid disentangled representation learning, where D can be any proper distance function such as mean square error. β -TCVAE proposed by [7] modifies the D_{KL} used in VAE into three part: *total correlation*, *index-coded mutual information* and *dimension-wise KL divergence*. To overcome the challenge proposed by [22], **AdaVAE** [23] purposely chooses pairs of inputs as supervision signal to learn representation disentanglement.

Invariant Representation Learning: The methods that aim at learning invariant representation can be classified into two groups: those methods that require annotations of nuisance factors [21,25] and those that do not. A considerable number of approaches using nuisance factors annotations have been recently proposed. By implementing a regularizer which minimizes the Maximum Mean Discrepancy (MMD) on neural network (NN), The **NN+MMD** approach [21] removes affects of nuisance from predictive factors. On the basis of **NN+MMD**, The Variational Fair Autoencoder (**VFAE**) [25]

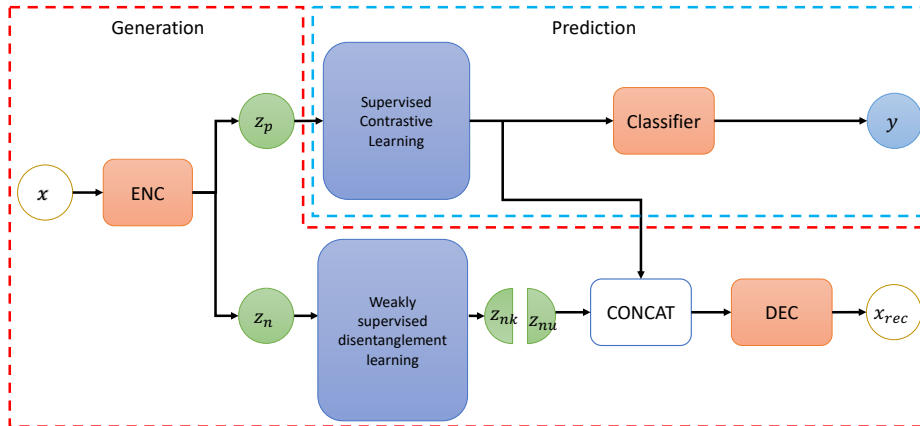


Fig. 2: Architecture of the model. Red box is the generation part and the blue box is the prediction part. Generation module aims at learning and splitting known nuisance factors z_{nk} and z_{nu} , and the prediction module aims at learning good predictive factors z_p .

uses special priors which encourage independence between nuisance factors and ideal invariant factors. The Controllable Adversarial Invariance (CAI) [32] approach applies the gradient reversal trick [9] which penalizes the model if latent representation has information of nuisance factors. CVIB [26] proposes a conditional form of Information Bottleneck (IB) and encourages the invariant representation learning by optimizing its variational bounds.

However, due to the constrains of demanding annotations, those methods take more effort to pre-process the data and encounter challenges when the annotations are inaccurate or insufficient. Comparing to annotation-eager approaches, annotation-free methods are easier to be implemented in practice. The Unsupervised Adversarial Invariance (UAI) [14] splits the latent factors into factors useful for prediction and nuisance factors. UAI encourages the independence of those two latent factors by incorporating competition between the prediction and the reconstruction objectives. NN+DIM [28] achieves invariant representation by using pairs of inputs and applying a neural network based mutual information estimator to minimize the mutual information between two shared representations. Furthermore, Sanchez *et al.* [28] employ a discriminator to distinguish the difference between shared representation and nuisance representation.

3 Learning disentangled and invariant representation

3.1 Model Architecture

As illustrated in Figure 2, the architecture of the proposed model contains two components: a generation module and a prediction module. Similar to VAE, the generation module performs the encoding-decoding task. However, it encodes the input x into latent factors z , $z = [z_p, z_n]$, where z_p represents the latent predictive factors that contains useful information for the prediction task, whereas z_n represents the latent nuisance

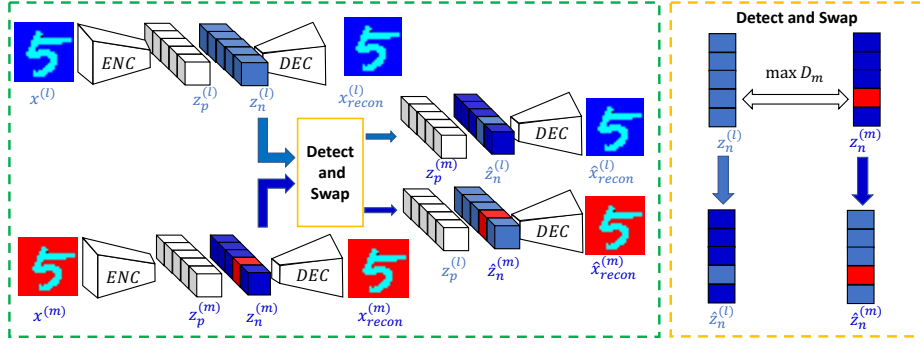


Fig. 3: Weakly supervised disentanglement representation learning for known nuisance factors z_{nk}

factors and can be further divided into known latent factors z_{nk} and unknown nuisance factors z_{nu} .

z_{nk} are discovered and separated from z_n via weakly supervised disentangled representation learning, where the joint distribution $p(z_{nk}) = \prod_i p(z_{nk_i})$. Since z_n is the split containing nuisance factor, after z_{nk} is identified, the remaining factors of z_n naturally result in unknown nuisance factors z_{nu} . Then, z_p and z_n are concatenated for generating reconstructions x_{rec} which are used to measure the quality of reconstruction. To enforce the independence between z_p and z_n , we add a regularizer using another reconstruction task, where the average mean and variance of predictive factors z_p are used to form new latent factors \bar{z}_p and it will be discussed in Section 3.3. In the prediction module, we further incorporate contrastive loss to cluster the predictive latent factors belonging to the same class.

3.2 Learning independent known nuisance factors z_{nk}

As illustrated in Figure 2, the known nuisance factors z_{nk} are discovered and separated from z_n , where $p(z_{nk}) = \prod_i p(z_{nk_i})$, since nuisance information is expected to be present only within z_n .

To fulfill the theoretical requirement of including supervision signal for disentangled representation learning as proven in [22], we use selected pairs of inputs $x^{(l)}$ and $x^{(m)}$ as supervision signals, where only a few common generative factors are shared. As illustrated in Figure 3, during training, the network encodes a pair of inputs $x^{(l)}$ and $x^{(m)}$ into two latent factors $z^{(l)} = [z_p^{(l)}, z_n^{(l)}]$ and $z^{(m)} = [z_p^{(m)}, z_n^{(m)}]$ respectively, which are then decoded to reconstruct $x_{rec}^{(l)}$ and $x_{rec}^{(m)}$. To encourage representation disentanglement, certain elements of $z_n^{(l)}$ and $z_n^{(m)}$ are *detected and swapped* to generate two new corresponding latent factors $\hat{z}^{(l)}$ and $\hat{z}^{(m)}$. The two new latent factors are then decoded to new reconstructions $\hat{x}_{rec}^{(l)}$ and $\hat{x}_{rec}^{(m)}$. By comparing \hat{x}_{rec} with x_{rec} , the known nuisance factors z_{nk} are discovered and the elements of z_{nk} are enforced to be mutually independent with each other.

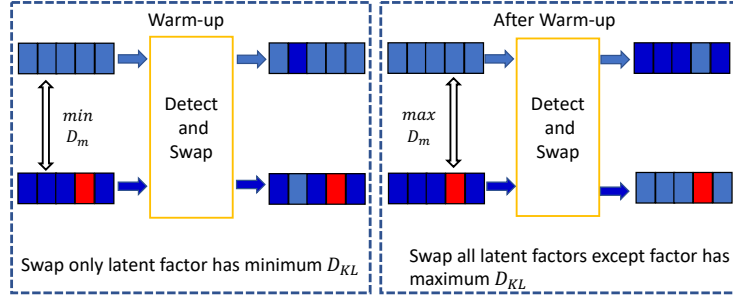


Fig. 4: In early training stages, small number of latent factors are swapped. the number of latent factors to be swapped increases gradually.

Selecting image pairs for training and latent factors assumptions: As mentioned by [13], the true world simulator using generative factors to generate x can be modeled as: $p(x|v, w) = Sim(v, w)$, where v is the generative factors and w is other nuisance factors. Inspired by this, we choose pairs of images by randomly selecting several generative factors to be the same and keeping the value of other generative factors to be random. Each image x has corresponding generative factors v , and the training pair is generated as follows: we first randomly select a sample $x^{(l)}$ whose generative factors are $v^{(l)} = [v_1, v_2, \dots, v_n]$. We then randomly change the value of k elements in $v^{(l)}$ to form a new generative factors $v^{(m)}$ and choose another sample $x^{(m)}$ according to $v^{(m)}$. During training, indices of different generative factors between $v^{(l)}$ and $v^{(m)}$, and the groundtruth value of all generative factors are not available to the model. The model is weakly supervised since it is trained with only the knowledge of the number of factors k that have changed. Ideally, if the model can learn a disentangled representation, the model will encode the image pair $x^{(l)}$ and $x^{(m)}$ to the corresponding representations $z^{(l)}$ and $z^{(m)}$ which have the characteristic shown in Equation (2). We annotate the set of all different elements between $z^{(l)}$ and $z^{(m)}$ to be df_z and set of all latent factors to be d_z such that $df_z \subseteq d_z$.

$$\begin{aligned} p(z_{n_j}^{(l)} | \mathbf{x}^{(l)}) &= p(z_{n_j}^{(m)} | \mathbf{x}^{(m)}); j \notin df_z \\ p(z_{n_i}^{(l)} | \mathbf{x}^{(l)}) &\neq p(z_{n_i}^{(m)} | \mathbf{x}^{(m)}); i \in df_z \end{aligned} \quad (2)$$

Detecting and Swapping the distinct latent factors: VAE adopts the reparameterization to make posterior distribution $q_\theta(z|x)$ differentiable, where the posterior distribution of latent factors is commonly assumed to be a factorized multivariate Gaussian: $p(z|x) = q_\theta(z|x)$ [17]. By this assumption, we can directly measure the mutual information between the corresponding dimensions of the two latent representations $z^{(l)}$ and $z^{(m)}$ by measuring the divergence (D_m), which can be KL divergence (D_{KL}). We show the process of detecting distinct latent factors in Equation (3), where a larger value of D_{KL} implies higher difference between the two corresponding latent factor distributions.

$$D_{KL}(q_\phi(z_i^{(l)} | x^{(l)}) || q_\phi(z_i^{(m)} | x^{(m)})) = \frac{(\sigma_i^{(l)})^2 + (\mu_i^{(l)} - \mu_i^{(m)})^2}{2(\sigma_i^{(l)})^2} + \log\left(\frac{\sigma_i^{(l)}}{\sigma_i^{(m)}}\right) - \frac{1}{2} \quad (3)$$

Since the model only has the knowledge of the number of different generative factors k , we swap all corresponding dimension elements of $z_n^{(l)}$ and $z_n^{(m)}$ except the top k highest D_m value elements. We incorporate this swapping step to create two new latent representations $\hat{z}_n^{(l)}$ and $\hat{z}_n^{(m)}$ shown in Equation (4).

$$\begin{aligned} \hat{z}_{n_i}^{(l)} &= z_{n_i}^{(m)}; \hat{z}_{n_i}^{(m)} = z_{n_i}^{(l)}; i \notin df_z \\ \hat{z}_{n_j}^{(l)} &= z_{n_j}^{(l)}; \hat{z}_{n_j}^{(m)} = z_{n_j}^{(m)}; j \in df_z \end{aligned} \quad (4)$$

Disentangled representation loss function: After $\hat{z}_n^{(l)}$ and $\hat{z}_n^{(m)}$ are obtained, they are concatenated with $z_p^{(m)}$ and $z_p^{(l)}$ respectively, to generate two new latent representations $\hat{z}^{(l)} = [z_p^{(m)}, \hat{z}_n^{(l)}]$ and $\hat{z}^{(m)} = [z_p^{(l)}, \hat{z}_n^{(m)}]$. $\hat{z}^{(l)}$ and $\hat{z}^{(m)}$ are decoded into new reconstructions $\hat{x}^{(l)}$ and $\hat{x}^{(m)}$. Since there are only k different generative factors between pair of images, ideally, after encoding the images, there should also be merely k pairs of different distributions on the latent representation space. By swapping other latent factors except them, the new representations $\hat{z}^{(l)}$ and $\hat{z}^{(m)}$ are the same with the original representations $z^{(l)}$ and $z^{(m)}$. Accordingly, the new reconstructions $\hat{x}_{rec}^{(l)}$ and $\hat{x}_{rec}^{(m)}$ should be identical to the original reconstruction $x_{rec}^{(l)}$ and $x_{rec}^{(m)}$. Therefore, we design the disentangled representation loss in Equation (5), where D can be any suitable distance function *e.g.*, mean square error (MSE) or binary cross-entropy (BCE).

$$L = L_{VAE}(x_{rec}^{(l)}, z^{(l)}) + L_{VAE}(x_{rec}^{(m)}, z^{(m)}) + D(\hat{x}_{rec}^{(l)}, x_{rec}^{(l)}) + D(\hat{x}_{rec}^{(m)}, x_{rec}^{(m)}) \quad (5)$$

Training Strategies for disentangled representation learning: To further improve the performance of disentangled representation learning, we design two strategies: *warmup by amount* and *warmup by difficulty*. Recalling that in the swapping step, the model needs to swap $|d_z| - k$ elements of latent representations. At beginning, exchanging too many latent factors will easily lead to mistakes. Therefore, in the first strategy, we gradually increase the number of latent factors being swapped from 1 to $|d_z| - k$. Further, to smoothly increase the training difficulty, we set the number of different generative factors to be 1 at the beginning and increase the number of different generative factors as training continues.

3.3 Learning invariant predictive factors z_p

After we obtain the disentangled representation z_{nk} , the predictive factors z_p may still be entangled with z_{nu} . Therefore, we need to add other constraints to achieve fully invariant representation of z_p .

Making z_p independent of z_n : As shown in [22], supervision signals need to be introduced for disentangled representation. Similarly, the independency of z_p and z_n also needs the help from a supervision signals as we discuss in Appendix. Luckily, for supervised training, a batch of samples naturally contains supervision signal. Similar to

Equation (2), the distribution of the representations z_p should be the same for the same class and can be shown in Equation (6) where $C(x^{(l)})$ means the class of sample $x^{(l)}$.

$$\begin{aligned} p(z_p^{(l)}|\mathbf{x}^{(l)}) &= p(z_p^{(m)}|\mathbf{x}^{(m)}); C(x^{(l)}) = C(x^{(m)}) \\ p(z_p^{(l)}|\mathbf{x}^{(l)}) &\neq p(z_p^{(m)}|\mathbf{x}^{(m)}); C(x^{(l)}) \neq C(x^{(m)}) \end{aligned} \quad (6)$$

Similar to the method we use for disentangled representation learning, we generate a new latent representation \tilde{z}_p and its corresponding reconstruction \tilde{x}_{rec-p} . Then, we enforce the disentanglement between z_p and z_n by comparing the new reconstruction \tilde{x}_{rec-p} and x_{rec} . In contrast to the swapping method mentioned in Section 3.2, since the batch of samples used for training often contains more than two samples from the same class, the swapping method is hard to be implemented in this situation. Therefore, we generate the new latent representations \tilde{z}_p by calculating the average mean $\bar{\mu}_p$ and average variance \bar{V}_p of the latent representations from the same class as shown in Equation (7).

$$\begin{aligned} \tilde{z}_p &= \mathcal{N}(\bar{\mu}_p, \bar{V}_p); \tilde{x}_{rec-p} = \text{Decoder}([\tilde{z}_p, z_n]) \\ \bar{\mu}_p &= \frac{1}{|C|} \sum \mu_p^{(i)}; \bar{V}_p = \frac{1}{|C|} \sum V_p^i, \text{ where } \forall i \in C \end{aligned} \quad (7)$$

We then generate the new reconstruction \tilde{x}_{rec-p} using the same decoder as in other reconstruction tasks and enforce the disentanglement of z_p and z_n by calculating the $D(x_{rec}, \tilde{x}_{rec-p})$ and update the parameters of the model according to its gradient.

Contrastive feature alignment: To achieve invariant representation, we need to make sure the latent representation that is useful for prediction can also be clustered according to their corresponding classes. Even though the often used cross-entropy (CE) loss can accomplish similar goals, the direct goal of CE loss is to achieve logit-level alignment and change the representations distribution according to the logits, which does not guarantee the uniform distribution of features. Alternatively, we incorporate contrastive methods to ensure that representation/feature alignment can be accomplished effectively [31].

Similar to [15], we use supervised contrastive loss to achieve feature alignment and cluster the representations z_p according to their classes as shown in Equation (8) where C is the set that contains samples from the same class and $y_p = y_i$.

$$\mathcal{L}_{sup} = \sum_{i \in I} \frac{-1}{|C|} \sum_{p \in C} \log \frac{\exp(z_i \cdot z_p / \tau)}{\sum_{a \in A(i)} \exp(z_i \cdot z_a / \tau)} \quad (8)$$

The final loss function used to train the model, after adding the standard cross-entropy(CE) loss to train the classifier, is given by Equation (9).

$$\begin{aligned} L &= L_{CE}(x, y) + L_{VAE} + \alpha L_{disentangle} + \beta L_{Sup} + \gamma L_{Z_p} \\ L_{disentangle} &= D(\hat{x}_{rec}^{(l)}, \hat{x}_{rec}^{(l)}) + D(\hat{x}_{rec}^{(m)}, \hat{x}_{rec}^{(m)}) \\ L_{Z_p} &= D(\tilde{x}_{rec-p}, x_{rec}) \end{aligned} \quad (9)$$

Table 1: Test average and worst accuracy results on Colored-MNIST, 3dShapes and MPI3D. **Bold, Black:** best result

Models	Colored-MNIST		3dShapes		MPI3D	
	Avg Acc	Worst Acc	Avg Acc	Worst Acc	Avg Acc	Worst Acc
Baseline	95.12 ± 2.42	66.17 ± 3.31	98.87 ± 0.52	96.89 ± 1.25	90.12 ± 3.13	87.89 ± 4.31
VFAE [25]	93.12 ± 3.07	65.54 ± 6.21	97.72 ± 0.81	93.34 ± 1.05	86.69 ± 3.12	82.43 ± 3.25
CAI [32]	93.56 ± 2.76	63.17 ± 5.61	97.62 ± 0.53	94.32 ± 0.89	86.63 ± 2.14	82.16 ± 5.83
CVIB [26]	93.31 ± 3.09	70.12 ± 4.77	97.11 ± 0.59	94.46 ± 0.90	87.04 ± 3.02	85.61 ± 2.08
UAI [14]	94.74 ± 2.19	74.25 ± 2.69	97.13 ± 1.02	95.21 ± 1.03	87.89 ± 4.23	83.01 ± 2.21
NN+DIM [28]	94.48 ± 2.35	80.25 ± 3.44	97.03 ± 1.07	96.02 ± 0.46	88.81 ± 1.37	82.01 ± 3.34
Our model	97.96 ± 1.21	90.43 ± 2.79	98.52 ± 0.51	97.63 ± 0.72	91.32 ± 2.38	89.17 ± 2.69

4 Experiments Evaluation

4.1 Benchmarks, Baselines and Metrics

The main objective of this work is to learn invariant representations and reduce overfitting to nuisance factors. Meanwhile, as a secondary objective, we also want to ensure that the learned representations are at least not less robust to adversarial attacks. Therefore, all models are evaluated on both invariant representation learning task and adversarial robustness task. We use four (4) dataset with different underlying factors of variations to evaluate the model:

- **Colored-MNIST** Colored-MNIST dataset is augmented version of MNIST [20] with two known nuisance factors: digit color and background color [28]. During training, the background color is chosen from three (3) colors and digit color is chosen from other six (6) colors. In test, we set the background color into three (3) new colors which is different from training set.
- **Rotation-Colored-MNIST** This dataset is further augmented version of Colored-MNIST. The background color and digit color setting is the same with the Colored-MNIST. This dataset further contains digits rotated to four (4) different angles $\Theta_{train} = \{0, \pm 22.5, \pm 45\}$. For test data, the rotation angles for digit is set to $\Theta_{test} = \{0, \pm 65, \pm 75\}$. The rotation angles are used as unknown nuisance factors.
- **3dShapes** [2] contains 480,000 RGB $64 \times 64 \times 3$ images and the whole dataset has six (6) different generative factors. We choose object shape (four (4) classes) as the prediction task and only half number of object colors are used during training, and the remaining half of object color samples are used to evaluate performance of invariant representation.
- **MPI3D** [10] is a real-world dataset contains 1,036,800 RGB images and the whole dataset has seven (7) generative factors. Like 3dShapes, we choose object shape (six (6) classes) as the prediction target and half of object colors are used for training.

Prediction accuracy is used to evaluate the performance of invariant representation learning. Furthermore, we record both average test accuracy and worst-case test accuracy which was suggested by [27]. We find that using Equation (9) directly does not

Table 2: Test average accuracy and worst accuracy results on Rotation-Colored-MNIST with different rotation angles. **Bold, Black**: best result

Models	Rotation-Colored-MNIST							
	Avg Acc	Worst Acc	Avg Acc	Worst Acc	Avg Acc	Worst Acc	Avg Acc	Worst Acc
	-75		-65		+65		+75	
Baseline	77.0 ±1.3	62.3 ±1.9	89.7 ±1.2	77.5 ±2.2	85.8 ±1.2	65.8 ±3.0	68.3 ±2.2	49.9 ±4.6
VFAE [25]	72.2 ±2.4	58.9 ±2.3	85.8 ±1.7	74.4 ±2.5	84.1 ±2.1	64.6 ±3.7	71.7 ±1.3	48.0 ±3.8
CAI [32]	74.9 ±0.9	59.3 ±3.9	86.5 ±1.9	77.3 ±2.0	84.2 ±1.7	67.8 ±1.9	64.7 ±4.2	42.9 ±3.7
CVIB [26]	76.1 ±0.8	59.2 ±3.0	88.6 ±0.9	79.1 ±1.2	85.6 ±0.7	68.8 ±2.9	72.2 ±1.2	53.4 ±2.6
UAI [14]	76.0 ±1.7	61.1 ±5.6	88.8 ±0.7	80.0 ±0.9	85.4 ±1.6	68.2 ±2.3	70.2 ±0.9	51.1 ±2.3
NN+DIM [28]	77.6 ±2.6	69.2 ±2.7	85.2 ±3.4	76.3 ±4.3	84.6 ±3.1	66.7 ±3.7	68.4 ±3.1	53.2 ±5.6
Our model	81.0 ±2.1	75.3 ±2.5	90.8 ±1.6	85.7 ±2.4	87.3 ±2.5	82.3 ±2.1	73.2 ±2.3	63.3 ±2.9

guarantee good performance. This may be caused by inconsistent behavior of CE loss and supervised contrastive loss. Thus, we separately train the classifier using CE loss and use remaining part of total loss to train the rest of the model.

Meanwhile, the performance of representation disentanglement is also important for representation invariance since it can evaluate the invariance of latent factors representing known nuisance factors.

We adopt the following metrics to evaluate the performance of disentangled representation. All metrics range from 0 to 1, where 1 indicates that the latent factors are fully disentangled — (1) **Mutual Information Gap (MIG)** [7] evaluates the gap of top two highest mutual information between a latent factors and generative factors. (2) **Separated Attribute Predictability (SAP)** [18] measures the mean of the difference of perdition error between the top two most predictive latent factors. (3) **Interventional Robustness Score (IRS)** [30] evaluates reliance of a latent factor solely on generative factor regardless of other generative factors. (4) **FactorVAE (FVAE) score** [16] implements a majority vote classifier to predict the index of a fixed generative factor and take the prediction accuracy as the final score value. (5) **DCI-Disentanglement (DCI)** [8] calculates the entropy of the distribution obtained by normalizing among each dimension of the learned representation for predicting the value of a generative factor.

4.2 Comparison with Previous Work

We show invariance learning results which are the test average accuracy and worst accuracy in Tables 1 and 2. For Color-Rotation-MNIST dataset, since we rotate the test samples with $\theta \in \Theta_{test} = \{\pm 65, \pm 75\}$ and those angles are different with training rotation angles $\theta \in \Theta_{train} = \{0, \pm 22.5, \pm 45\}$, we record each average accuracy and worst accuracy under each rotation angles. The baseline model is the regular VGG16 model with no extra components for representation invariance. Our model largely outperforms prior work.

To compare the performance of disentanglement, we show the results of disentanglement representation learning in Table 3. Since the Color-MNIST and Rotation-Color-MNIST have only two generative factors, models for disentanglement learning

Table 3: Disentanglement metrics on 3dShapes and MPI3D. **Bold, Black**: best result

Models	3dShapes					MPI3D				
	MIG	SAP	IRS	FVAE	DCI	MIG	SAP	IRS	FVAE	DCI
Unsupervised Disentanglement Learning										
β -VAE [13]	0.194	0.063	0.473	0.847	0.246	0.135	0.071	0.579	0.369	0.317
AnnealedVAE [3]	0.233	0.087	0.545	0.864	0.341	0.098	0.038	0.490	0.397	0.228
FactorVAE [16]	0.224	0.0440	0.630	0.792	0.304	0.092	0.031	0.529	0.379	0.164
DIP-VAE-I [18]	0.143	0.026	0.491	0.761	0.137	0.104	0.073	0.476	0.491	0.223
DIP-VAE-II [18]	0.137	0.020	0.424	0.742	0.083	0.131	0.075	0.509	0.544	0.244
β -TCVAE [7]	0.364	0.096	0.594	0.970	0.601	0.189	0.146	0.636	0.430	0.322
Weakly-Supervised Disentanglement Learning										
Ada-ML-VAE [23]	0.509	0.127	0.620	0.996	0.940	0.240	0.074	0.576	0.476	0.285
Ada-GVAE [23]	0.569	0.150	0.708	0.996	0.946	0.269	0.215	0.604	0.589	0.401
Our model	0.716	0.156	0.784	0.996	0.919	0.486	0.225	0.615	0.565	0.560

tends to achieve nearly perfect disentanglement metric scores, which makes the results seems trivial. Therefore, we only record the disentanglement scores tested on **3dshapes** and **MPI3D** datasets.

To test the ability to defend adversarial attack without adversarial augmentation, we first train all models on **Colored-MNIST**, **CIFAR10** and **CIFAR100**. Then, we apply different adversarial attacks on those datasets. The adversarial attack types are: Fast Gradient Sign Method (FGSM) attack [11], Projected Gradient Descent (PGD) attack [19], and Carlini & Wagner (C&W) attack [4]. FSGM and PGD attacks results are shown in Figure 5 and C&W attack results are included Appendix.

Table 4: Disentanglement metrics of with different training strategies applied to 3dShapes

	warmup by amount	warmup by difficulty	MIG	SAP	IRS	FVAE	DCI
			0.492	0.096	0.661	0.902	0.697
	✓		0.512	0.126	0.674	0.944	0.781
	✓	✓	0.716	0.156	0.784	0.996	0.919

4.3 Ablation Study

Effectiveness of training strategies in disentanglement learning: To prove the effectiveness of the training strategies illustrated in Figure 4, we compare results of three situations: (1) none of those strategies is used, (2) only *warmup by amount* strategy is used, and (3) both strategies are used. As shown in Table 4, using both training strategies clearly outperforms the others.

Table 5: Performance of different scheme on Colored-MNIST and Rotation-Colored-MNIST

Training Scheme	Colored-MNIST		Rotation-Colored-MNIST (65)	
	avg acc	worst acc	avg acc	worst acc
L_{CE}	0.932	0.680	0.821	0.653
$L_{CE} + L_{contrastive}$	0.935	0.732	0.842	0.678
$L_{CE} \leftrightarrow L_{contrastive}$	0.980	0.904	0.873	0.823

Separately training the classifier and the rest of the model: To prove the importance of the two-step training as mentioned in Section 4.1, we compare the results of training the entire model together versus separately training classifier and other parts. Further, we also record the results of our model which does not use contrastive loss for feature-level alignment. As shown in Table 5, either only using CE loss (L_{CE}) or training the whole together ($L_{CE} + L_{contrastive}$) will harm the performance of the model. By separately training the classifier and other parts ($L_{CE} \leftrightarrow L_{contrastive}$), the framework has the best results for both average and worst accuracy.

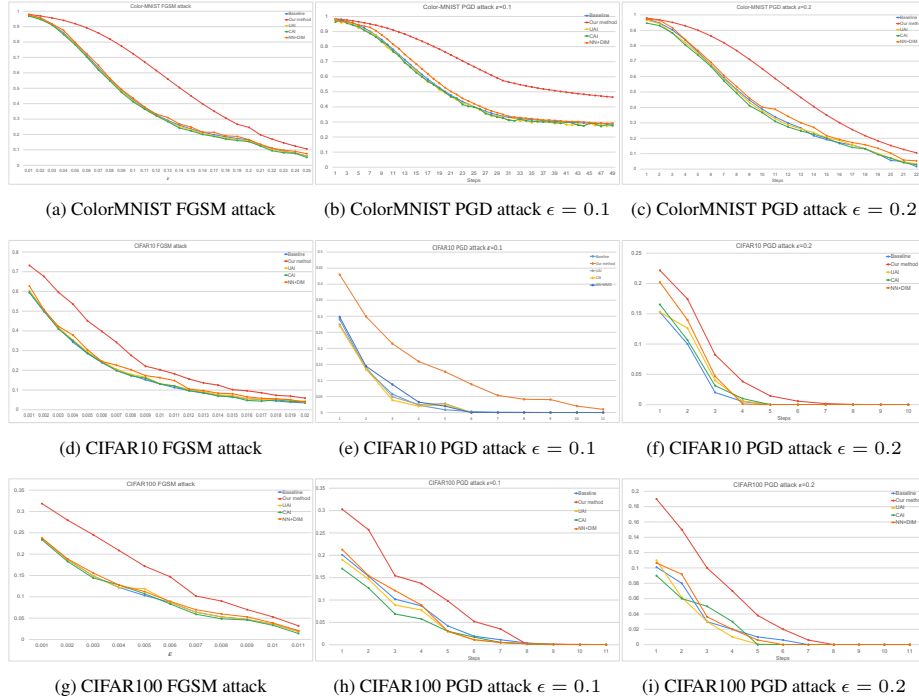


Fig. 5: FGSM attacks and PGD attacks results

5 Conclusion

In this work, we extend the ideas of representation disentanglement and representation invariance by combining them to achieve both goals at the same time. By introducing contrastive loss and new invariant regularization loss, we make predictive factor z_p to be more invariant to nuisance and increase both average and worst accuracy on invariant learning tasks. Furthermore, we demonstrate that simultaneously achieving invariant and disentangled representation can increase the performance of adversarial defense comparing to merely using invariant representation learning.

Acknowledgement: This research is based upon work supported by the Defense Advanced Research Projects Agency (DARPA), under cooperative agreement number HR00112020009. The views and conclusions contained herein should not be interpreted as necessarily representing the official policies or endorsements, either expressed or implied, of DARPA or the U.S. Government. The U.S. Government is authorized to reproduce and distribute reprints for governmental purposes notwithstanding any copyright notation thereon.

References

1. Bengio, Y., Courville, A., Vincent, P.: Representation learning: A review and new perspectives (2014)
2. Burgess, C., Kim, H.: 3d shapes dataset. <https://github.com/deepmind/3dshapes-dataset/> (2018)
3. Burgess, C.P., Higgins, I., Pal, A., Matthey, L., Watters, N., Desjardins, G., Lerchner, A.: Understanding disentangling in β -vae (2018)
4. Carlini, N., Wagner, D.: Towards evaluating the robustness of neural networks. In: 2017 IEEE Symposium on Security and Privacy (SP) (2017)
5. Castro, P.S.: Scalable methods for computing state similarity in deterministic markov decision processes. In: AAAI (2020)
6. Chen, J., Konrad, J., Ishwar, P.: A cyclically-trained adversarial network for invariant representation learning. In: CVPR Workshops (2020)
7. Chen, R.T.Q., Li, X., Grosse, R., Duvenaud, D.: Isolating sources of disentanglement in variational autoencoders (2019)
8. Eastwood, C., Williams, C.K.I.: A framework for the quantitative evaluation of disentangled representations. In: ICLR (2018), <https://openreview.net/forum?id=By-7dz-AZ>
9. Ganin, Y., Ustinova, E., Ajakan, H., Germain, P., Larochelle, H., Laviolette, F., Marchand, M., Lempitsky, V.: Domain-adversarial training of neural networks. *The Journal of Machine Learning Research* (2016)
10. Gondal, M.W., Wüthrich, M., Đorđe Miladinović, Locatello, F., Breidt, M., Volchkov, V., Akpo, J., Bachem, O., Schölkopf, B., Bauer, S.: On the transfer of inductive bias from simulation to the real world: a new disentanglement dataset (2019)
11. Goodfellow, I.J., Shlens, J., Szegedy, C.: Explaining and harnessing adversarial examples (2014), <http://arxiv.org/abs/1412.6572>, cite arxiv:1412.6572
12. He, K., Zhang, X., Ren, S., Sun, J.: Deep residual learning for image recognition (2015)
13. Higgins, I., Matthey, L., Pal, A., Burgess, C., Glorot, X., Botvinick, M., Mohamed, S., Lerchner, A.: beta-vae: Learning basic visual concepts with a constrained variational framework. In: ICLR (2017)

14. Jaiswal, A., Wu, R.Y., Abd-Almageed, W., Natarajan, P.: Unsupervised adversarial invariance. In: *Advances in Neural Information Processing Systems* 31 (2018)
15. Khosla, P., Teterwak, P., Wang, C., Sarna, A., Tian, Y., Isola, P., Maschinot, A., Liu, C., Krishnan, D.: Supervised contrastive learning. *CoRR* **abs/2004.11362** (2020), <https://arxiv.org/abs/2004.11362>
16. Kim, H., Mnih, A.: Disentangling by factorising. In: *ICML* (2018), <http://proceedings.mlr.press/v80/kim18b.html>
17. Kingma, D.P., Welling, M.: Auto-encoding variational bayes. In: *ICLR* (2014)
18. Kumar, A., Sattigeri, P., Balakrishnan, A.: Variational inference of disentangled latent concepts from unlabeled observations. *ICLR* (2018)
19. Kurakin, A., Goodfellow, I.J., Bengio, S.: Adversarial machine learning at scale. *CoRR* **abs/1611.01236** (2016), <http://arxiv.org/abs/1611.01236>
20. LeCun, Y., Cortes, C.: MNIST handwritten digit database (2010), <http://yann.lecun.com/exdb/mnist/>
21. Li, Y., Swersky, K., Zemel, R.: Learning unbiased features. *arXiv preprint arXiv:1412.5244* (2014)
22. Locatello, F., Bauer, S., Lucic, M., Rätsch, G., Gelly, S., Schölkopf, B., Bachem, O.: Challenging common assumptions in the unsupervised learning of disentangled representations (2019)
23. Locatello, F., Poole, B., Raetsch, G., Schölkopf, B., Bachem, O., Tschannen, M.: Weakly-supervised disentanglement without compromises. In: *ICML* (2020), <http://proceedings.mlr.press/v119/locatello20a.html>
24. Locatello, F., Tschannen, M., Bauer, S., Rätsch, G., Schölkopf, B., Bachem, O.: Disentangling factors of variations using few labels. In: *ICLR* (2020), <https://openreview.net/forum?id=SygagpEKwB>
25. Louizos, C., Swersky, K., Li, Y., Welling, M., Zemel, R.: The variational fair autoencoder. In: *ICLR* (2016)
26. Moyer, D., Gao, S., Brekelmans, R., Galstyan, A., Ver Steeg, G.: Invariant representations without adversarial training. In: *Advances in Neural Information Processing Systems* 31 (2018)
27. Sagawa*, S., Koh*, P.W., Hashimoto, T.B., Liang, P.: Distributionally robust neural networks. In: *ICLR* (2020), <https://openreview.net/forum?id=ryxGuJrFvS>
28. Sanchez, E., Serrurier, M., Ortner, M.: Learning disentangled representations via mutual information estimation. In: *ECCV* (2020)
29. van Steenkiste, S., Locatello, F., Schmidhuber, J., Bachem, O.: Are disentangled representations helpful for abstract visual reasoning? *CoRR* **abs/1905.12506** (2019), <http://arxiv.org/abs/1905.12506>
30. Suter, R., Đorđe Miladinović, Schölkopf, B., Bauer, S.: Robustly disentangled causal mechanisms: Validating deep representations for interventional robustness (2019)
31. Wang, F., Liu, H.: Understanding the behaviour of contrastive loss. In: *CVPR* (2021)
32. Xie, Q., Dai, Z., Du, Y., Hovy, E., Neubig, G.: Controllable invariance through adversarial feature learning. In: *Advances in Neural Information Processing Systems* 30 (2017)

6 Appendix

6.1 Why reconstruction job is necessary for independent predictive factors

This proof is largely dependent on proof used in [22] and the proof is shown below:

By the assumption, we hope the latent factors can be separated into two part z_p and z_n . z_p and z_n are expected to be independent to each other. We have :

$$p(z) = p(z_p) \cdot p(z_n)$$

Thus, if we choose any latent factor z_i from z_p , it should be independent to any other latent factor z_j chosen from z_n . $z_i \perp\!\!\!\perp z_j$.

It can be claimed that there exists an infinite family of bijective functions $f : \text{supp}(z) \rightarrow \text{supp}(z)$ such that $\frac{\partial f_i(u)}{\partial u_j} \neq 0$ almost everywhere for all i in z_p and j from z_n (i.e., z and $f(z)$ are completely entangled) and $P(z \leq u) = P(f(z) \leq u)$ for all $u \in \text{supp}(z)$ (i.e., they have the same marginal distribution). Since the unsupervised method only has access to observations x and y , it hence cannot distinguish between the two equivalent generative models and thus has to be entangled to at least one of them.

We first choose two bijective functions $g_i(v_i) = P(z_i \leq v_i)$ and $g_j(v_j) = P(z_j \leq v_j)$. By construction $g(z) = g(z_i) \cdot g(z_j)$ is a 2-dimensional uniform distribution. Similarly, consider function $h_i(v_i) = \psi^{-1}(v_i)$ and $h_j(v_j) = \psi^{-1}(v_j)$. Where,

$\psi(\cdot)$ is the cumulative density function of standard normal distribution. By this further construction, the random variable $h(g(z))$ is a 2-dimensional standard normal distribution.

Let $A \in R^{2 \times 2}$ be an arbitrary orthogonal matrix with $A_{km} \neq 0$ for all $k = 1, 2$ and $m = 1, 2$. An infinite family of such matrices can be constructed using a Householder transformation: Choose an arbitrary $\alpha \in (0, 0.5)$ and consider the vector v with $v_1 = \sqrt{\alpha}$ and $v_2 = \sqrt{1 - \alpha}$. By construction, we have $\mathbf{v}^T \mathbf{v} = 1$. Define the matrix $A = \mathbf{I}_2 - 2\mathbf{v}\mathbf{v}^T$. Furthermore, A is orthogonal since

$$A^T A = (\mathbf{I}_2 - 2\mathbf{v}\mathbf{v}^T)^T (\mathbf{I}_2 - 2\mathbf{v}\mathbf{v}^T) = \mathbf{I}_2 - 4\mathbf{v}\mathbf{v}^T + 4\mathbf{v}(\mathbf{v}^T \mathbf{v})\mathbf{v}^T = \mathbf{I}_2$$

Since A is orthogonal, it is invertible and thus defines a bijective linear operator. The random variable $Ah(g(z)) \in R^2$ is hence an independent, multivariate standard normal distribution since the covariance matrix $A^T A$ is equal to I_2 .

Since h is bijective, it follows that $h^{-1}(Ah(g(z)))$ is an independent 2-dimensional uniform distribution. Define the function $f : \text{supp}(z) \rightarrow \text{supp}(z)$

$$f(u) = g^{-1}(h^{-1}(Ah(g(u))))$$

and note that by definition $f(z)$ has the same marginal distribution as z under P , i.e., $P(z \leq u) = P(f(z) \leq u)$ for all u . Finally, for almost every $u \in \text{supp}(z)$, it holds that

$$\frac{\partial f_i(u)}{\partial u_j} \neq 0,$$

Since A was chosen arbitrarily, there exists an infinite family of such function f .

To overcome this problem, we need to do similar reconstruction job like we do for disentangled representation learning, where introducing supervision signal to enforce independence between z_p and z_n is necessary. However, previous works [14,32,25,26] fail to do that. The detail of the process is described in Section 3.3.

6.2 Other Adversarial attack results

In this section, We record the Carlini & Wangner (C&W) attack results with varying initial constant c in Table 6.1.

Table 6.1: Carlini & Wangner (C&W) attack results

Model	Color-MNIST			CIFR10		CIFAR100
	c = 0.01	c = 0.1	c = 1	c = 0.01	c = 0.1	c = 0.01
Baseline	0.923	0.616	0.282	0.301	0.112	0.103
UAI [14]	0.916	0.607	0.279	0.310	0.083	0.097
CAI [32]	0.902	0.594	0.267	0.319	0.105	0.081
NN+DIM [28]	0.917	0.638	0.295	0.296	0.135	0.121
Our method	0.945	0.792	0.496	0.462	0.204	0.213

6.3 Visualization of latent space

To illustrate the performance of the results of the model, we visualize the latent representation by different methods. We first visualize the t-SNE results of z_p and z_{nu} which we tested on Color-Rotation-MNIST in Figure 6.1.

Further, we visualize the heatmap of latent space change by giving the model with different inputs. In Figure 6.2, we visualize the latent factors change of model tested on Colored-MNIST and visualize the latent factors change of model tested on Rotation-Colored-MNIST in Figure 6.3.

We finally visualize the results of reconstruction of model we tested on Colored-MNIST in Figure 6.4. Images in line 1-2 are original images used for training. Images in line 3-4 are reconstructions which are expected to be same with original inputs. Images in line 5-6 are reconstructions after swapping operation which are also expected to be same with original inputs and reconstruction in line 2-3. Images in line 7-8 are decoded from $[rand(z_p), z_n]$, where $rand(z_p)$ is normal random noise. Since we random sample z_p , the outputs of decoder should only contains the color information and unrecognized digits. In the contrary, images in line 9-10, we randomly sampled z_n and the latent factors for decoding is $[z_p, rand(z_n)]$. Therefore, images in line 9-10 should have same digit pattern with original inputs but have random digit color and background color. Besides, other nuisance factors like hand-writing style and dilated or eroded shapes will also change since z_n has split z_{nu} which contains unknown nuisance factors information.

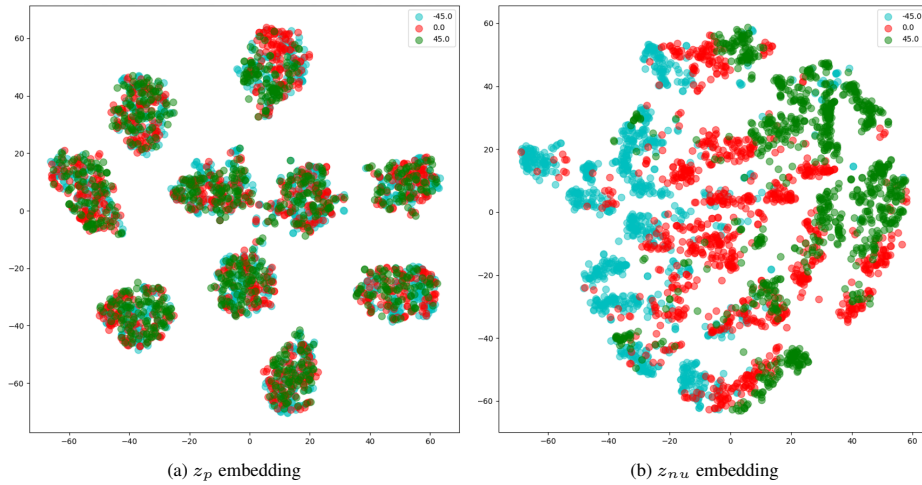


Fig. 6.1: t-SNE visualization of z_p and z_{nu} embeddings of Color-Rotation-MNIST images colored by rotation angle. As desired, the z_p embedding does not encode rotation information, which migrates to z_{nu} .

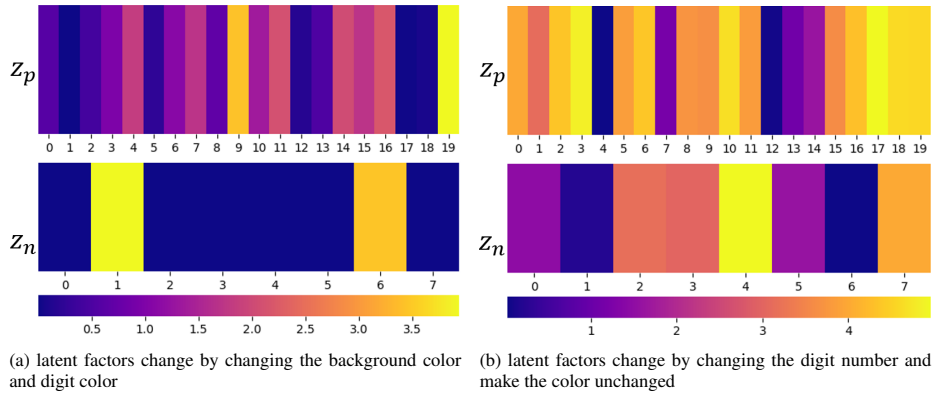


Fig. 6.2: Heat map visualization for Colored-MNIST dataset

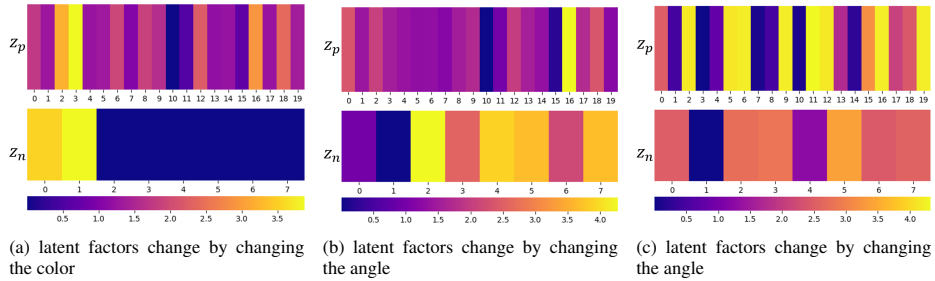


Fig. 6.3: Heat map visualization for Rotation-Colored-MNIST dataset

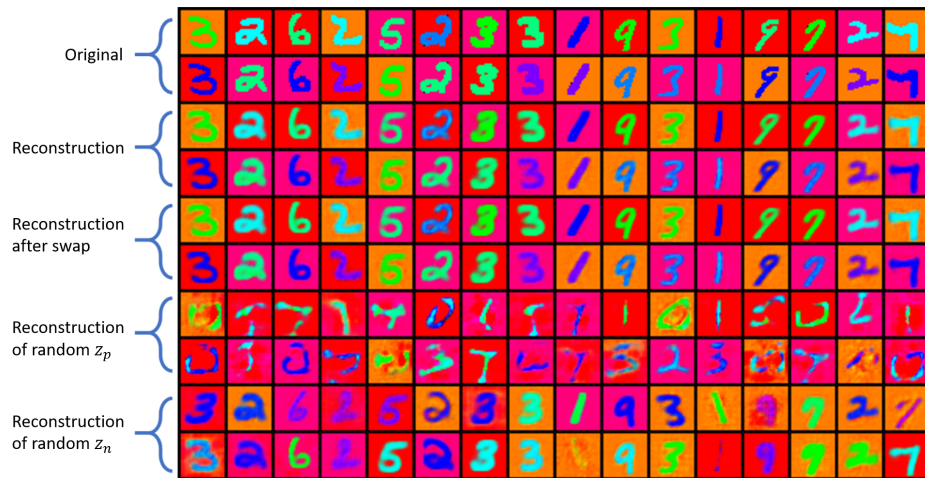


Fig. 6.4: Reconstruction results of Colored-MNIST data